# Submicro-sized $LiMn_2O_4$ prepared by a sol–gel, spray-drying method

CHUANYUN WAN, YANNA NULI, QIANG WU, MANMING YAN and ZHIYU JIANG*
*Department of Chemistry, Fudan University, Shanghai 200433, China*
*(*author for correspondence, e-mail: zyjiang@fudan.ac.cn)*

## Abstract

Submicro-sized $LiMn_2O_4$ powders were produced by a sol–gel, spray-drying method in which a brown gel precursor was prepared via the reaction of LiOH alkaline solution with 1 M $Mn(CH_3COO)_2$. The gel precursor was then transferred into a dry precursor powder via a spray-dry process. After heating treatment the spinel $LiMn_2O_4$ powder was obtained. The composition and the crystal size of the samples were strongly affected by the spray speed in the drying process and the heating temperature. The structure and the morphology of $LiMn_2O_4$ powder were investigated by DTA, TGA, IR, XRD and SEM methods. It was discovered that submicro-sized $LiMn_2O_4$ powder could be formed under the conditions of rotating spray speed of 15 000 rpm and syntheses temperature of 700 °C. The electrochemical properties of $LiMn_2O_4$ samples in 1 M $LiPF_6$, EC:DMC = 1:1 solution were tested by measuring the voltammograms and charge–discharge curves. The submicro-sized $LiMn_2O_4$ sample made at 700 °C has a capacity of 128 mAh $g^{-1}$ and good cycle stability for $Li^+$ intercalation reaction. This method may be applied to the industrial-scale production of superfine $LiMn_2O_4$ powder for use in lithium ion batteries.

## 1. Introduction

Spinel $LiMn_2O_4$ has received great attention as the cathodic material for rechargeable lithium ion batteries because of its low cost and low toxicity. $LiMn_2O_4$ powder is usually prepared by a solid-state reaction of lithium salt such as lithium hydroxide, carbonate, or nitrate with manganese compounds such as manganese oxide, hydroxide, or carbonate at a high temperature [1–7]. However, this method has several disadvantages: inhomogeneity, irregular morphology and the difficulty of controlling the $LiMn_2O_4$ particle size. Recently a sol–gel method was used to prepare a thin $LiMn_2O_4$ film [8, 9]. Nanocrystalline $LiMn_2O_4$ was prepared to produce solid-state thin-film rechargeable lithium batteries [10]. Some new dynamic processes were used to produce superfine $LiMn_2O_4$, $LiCoO_2$ powder for the use in lithium ion batteries, such as the airborne aerosol dynamic method [11] and the spray-drying method [12, 13]. In this paper a method for preparation of submicro-sized $LiMn_2O_4$ powder by using sol–gel, spray-drying method is introduced. The submicro-sized $LiMn_2O_4$ shows good electrochemical properties in a $Li^+$ intercalation reaction. The method is able to produce $LiMn_2O_4$ powder for practical use. The effect of temperature during the solid state reaction on the

electrochemical properties of the $LiMn_2O_4$ samples was also investigated.

## 2. Experimental details

### 2.1. *Preparation of spinel $LiMn_2O_4$ powder*

Two solutions, 1 M LiOH alkaline and 1 M $Mn(CH_3COO)_2$ were prepared to generate the gel precursors. The pH of the alkaline solution was adjusted to 7–8 by adding ammonia. The alkaline solution was added slowly to the 1 M $Mn(CH_3COO)_2$ solution with intense stirring. The solution was then stirred continuously for 2 h until a brown uniform gel precursor formed. The molecular ratio of Li:Mn in the precursor was 1:2. The reagents used were AR grade. The dry precursor powder was formed via a spray-dry process using the equipment shown in Figure 1. The gel was sprayed via a rotating sprinkler at the top of a spray-dry vessel, and the gel particles were dried inside this vessel in dry flowing air. The temperature at the entrance of the spray-dry vessel was 260–280 °C. The maximum rotating speed of the sprinkler was 50 000 rpm. The temperature at the exit for the collecting dry precursor powder was approximately 150 °C. Adjusting the rotation speed of the sprinkler controlled the size of the precursor powder
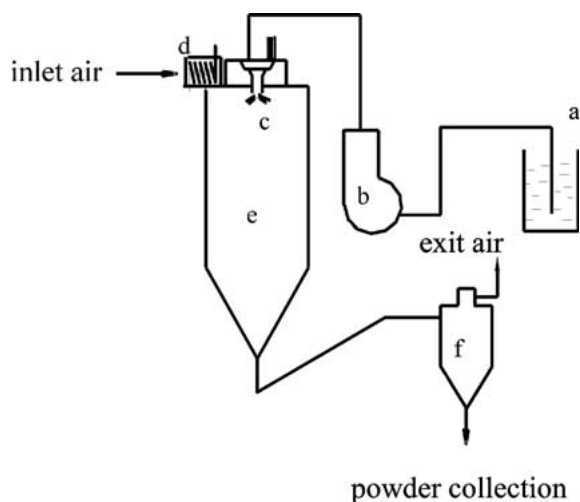
Fig. 1. Schematic overview of spray dryer equipment. (a) Gel precursor container; (b) pump; (c) sprinkler; (d) heater; (e) spray-dry vessel; (f) cyclone separator.

particles. After heat treatment in a resistance furnace in air the precursor $LiMn_2O_4$ powder was formed via a solid state reaction. The heating procedure was programmed so that the temperature rose at a rate of $1\ °C\ min^{-1}$ until a specified temperature was reached. The compound was then heated continuously for 12 h at that temperature.

Differential thermal analysis (DTA) and thermogravimetric analysis (TGA) were curried out by Perkin Elmer DTA7 and Perkin Elmer TGA7 analysers, respectively, to investigate the solid state reaction. A Nicolet 360 FTIR spectroscope and a Bruker D8 Advance X-ray diffractometer with $CuK_\alpha$ radiation were used to measure the structure characteristics of the samples. The morphology and the particle size of the samples were measured using a Philips XL30 microscope. The cyclic voltammetry of $LiMn_2O_4$ was evaluated in a three-chamber cell. The working electrode consisted of 80% (weight percent) active material $LiMn_2O_4$, 15% acetylene black and 5%PTFE binder. Each working electrode contained 5 mg $LiMn_2O_4$ and had a surface area of 0.5 cm$^2$. Both counter and reference electrodes were lithium sheets. The potentials presented in this paper correspond to the lithium electrode. The charge–discharge curves and the cyclic stability of the $LiMn_2O_4$ samples were evaluated in model CR2025 button cells, which consisted of a $LiMn_2O_4$-based positive electrode with the aforementioned composition, a metal lithium foil negative electrode and a Celgard 2300 membrane as separator. The amount of $LiMn_2O_4$ in the positive electrode was 20 mg. The electrolyte was 1 M $LiPF_6$ in a 1:1 (volume ratio) mixture of ethylene carbonate (EC) and dimethyl carbonate (DMC) (Merck). Cells were assembled in a dry box. The charge–discharge cycling was galvanostatically tested at a current density of 0.2 mA cm$^{-2}$, with cut-off voltages at 4.3 and 3.0 V for charge and discharge processes, respectively. The cyclic voltammetry experiments were curried out using a CHI660 electrochemical workstation at room temperature.

# 3. Results and discussion

## 3.1. Analysis of crystallinity and microstructure

### 3.1.1. IR spectra

Figure 2 represents the FTIR spectra of dry precursor powder after heat treatment at 150 °C (curve a) and 250 °C (curve b), respectively. Compare spectrum a with the spectrum of $Mn(CH_3COO)_2$ (curve c), most of the $Mn(CH_3COO)_2$ peaks appear on curve (a), which indicates that the substance $Mn(CH_3COO)_2$ contained in precursor almost did not decompose at 150 °C. After heat treatment at 250 °C, the spectrum (curve b) became totally different and demonstrated the characteristics of spinel $LiMn_2O_4$. Two main absorption bands appear at 502 cm$^{-1}$ and 620 cm$^{-1}$. These bands are attributed to the vibrations of Mn–O–Mn bands in Octahedral $MO_6$ units [14]. The results suggest that spinel $LiMn_2O_4$ can be synthesized at a relative low temperature in sol–gel spray-drying method.
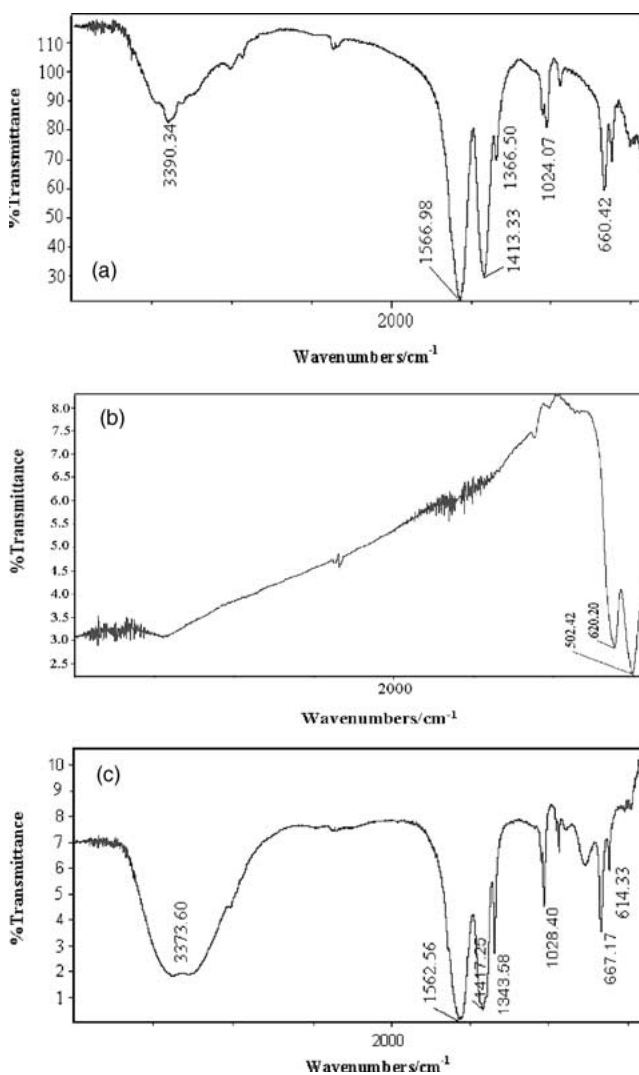


Fig. 2. Infrared spectra of the precursor powders treated for 12 h at (a) 150 °C and (b) 250 °C; (c) infrared spectrum of Mn $(CH_3COO)_2$.

### 3.1.2. Thermal analysis

The results of differential thermal analysis (DTA) and thermogravimetric analysis (TGA) for dry precursor powder in nitrogen atmosphere are shown in Figure 3. In the temperature range 50–200 °C, the weight loss and the simultaneous temperature decrease can be attributed to the evaporation of adsorbed water. A big weight loss occurs in the temperature range 210–350 °C, which reflects the presence of the solid state reaction that produces spinel $LiMn_2O_4$. The reaction may include three steps, because three downward endothermic $\Delta T$ peaks at 240 °C, 260 °C and 310 °C appear on the DTA curve. This hypothesis is in agreement with the observation by others [15].

### 3.1.3. XRD measurements

The result in studying the influence of heating temperature on the composition of the samples was confirmed by XRD measurement. Figure 4 shows the powder X-ray diffraction patterns of the samples synthesized at different temperatures. There is no diffraction peak on

Table 1. Intensity and half width of (1 1 1) XRD peak for $LiMn_2O_4$ samples synthesized at different temperatures

|  | 350 °C | 550 °C | 650 °C | 700 °C | 800 °C |
|---|---|---|---|---|---|
| Intensity of (1 1 1) peak/count | 236 | 242 | 419 | 653 | 487 |
| Width of (1 1 1) half peak/degree | 0.399 | 0.238 | 0.219 | 0.203 | 0.192 |

the XRD pattern for the sample treated at 150 °C, which indicates that the sample was basically amorphous. When the temperature rose above 250 °C, all of the curves showed the characteristics of spinel $LiMn_2O_4$ structure. $LiMn_2O_4$ samples of pure spinel structure can be produced by heat treatment at relatively high temperature. The result is in agreement with the observation of IR analysis described previously. Table 1 represents the influence of temperature on the intensity and the half peak width of (1 1 1) XRD peak of $LiMn_2O_4$ samples. Up to 700 °C, the peak intensities increase and wideness decreases with the rising
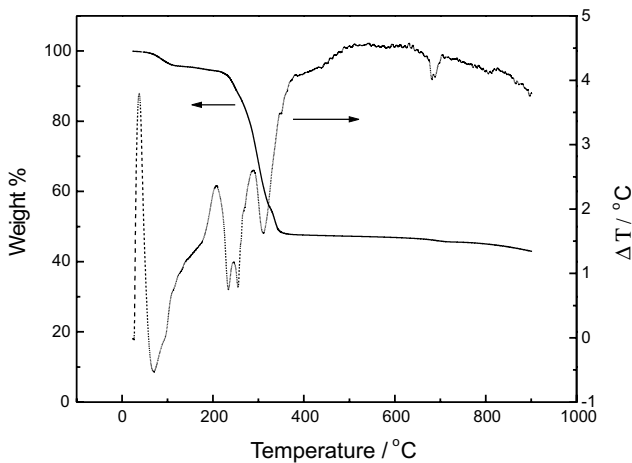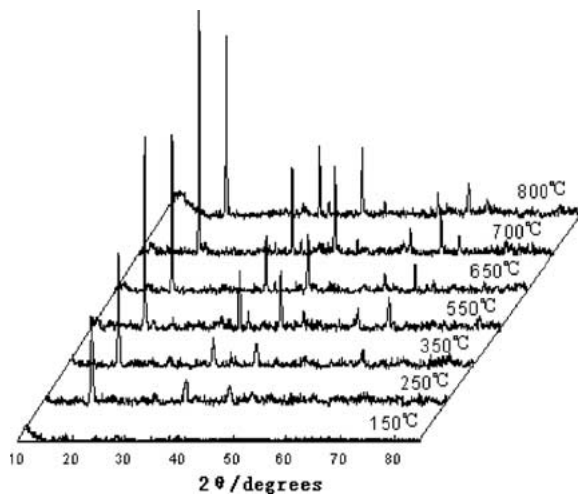
Fig. 3. DTA and TGA curves of dry precursor powder.

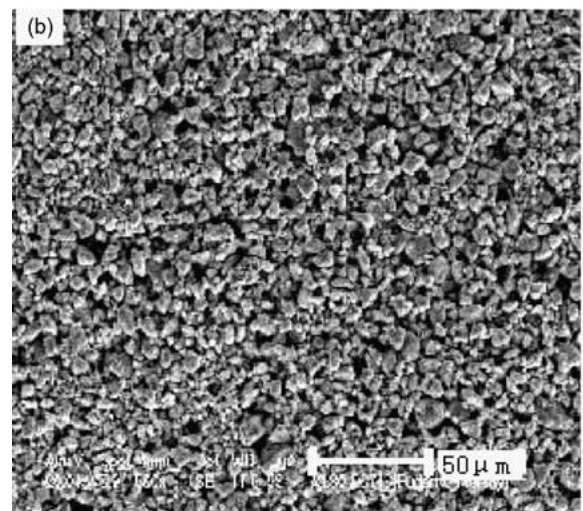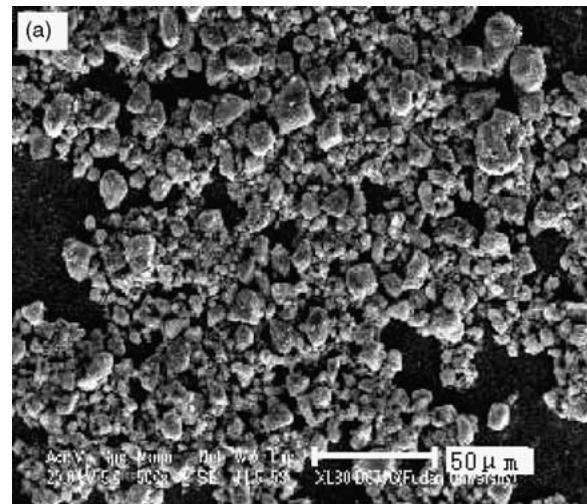Fig. 4. XRD patterns of the samples produced at the temperatures shown.

Fig. 5. SEM morphology of $LiMn_2O_4$ powder prepared at different conditions. Spraying speed 9000 rpm; temperature (a) 250 °C and (b) 700 °C.
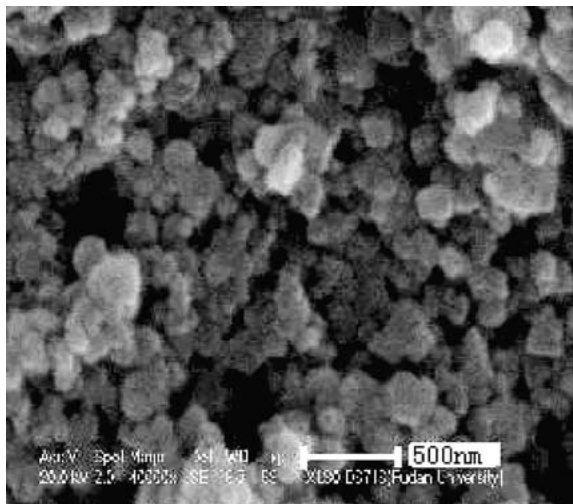
Fig. 6. SEM morphology of LiMn$_2$O$_4$ powder prepared at: spraying speed 9000 rpm and heat temperature 250 °C.

temperature. The intensity of the peaks reduced slightly when the temperature rose above 700 °C. It seems that 700 °C is the best synthesis temperature.

### 3.1.4. SEM analysis

The size of LiMn$_2$O$_4$ powder was affected mainly by the rotation speed of the sprinkler and the heating temperature. Figure 5 shows the morphology of LiMn$_2$O$_4$ samples prepared at spray speed of 9000 rpm and

temperature 250 °C (image a) or 700 °C (image b), respectively. It can be seen that the higher heating temperature, the smaller the crystal size. Figure 6 presents the morphology of LiMn$_2$O$_4$ sample formed in the case with rotation speed of 15 000 rpm and temperature 700 °C. From this image the diameter of submicro-sized LiMn$_2$O$_4$ crystal is in the range 100–200 nm. This shows that superfine crystal powder can be obtained by use of very fast rotating spray technology. Suitably sized LiMn$_2$O$_4$ particles can be obtained by control of the rotating spray speed and heating temperature.

### 3.2. Effects of heating temperature on the electrochemical properties of LiMn$_2$O$_4$

### 3.2.1. Cyclic voltammetry behaviour

The electrochemical properties of spinel LiMn$_2$O$_4$ are strongly affected by the heating process. Figure 7 presents the voltammograms of various LiMn$_2$O$_4$ samples obtained at the same sprinkler rotation speed of 15 000 rpm but different heating temperatures. The synthesis temperatures for curves (a)–(d) were 250, 650, 700 and 800 °C, respectively. All curves demonstrate the electrochemical characteristics of spinel LiMn$_2$O$_4$. Two couples of redox current peaks located at about 3.95 V/4.08 V and 4.05 V/4.20 V appear on each curve. They correspond to a two-step reversible intercalation reaction, in which lithium ions occupy two
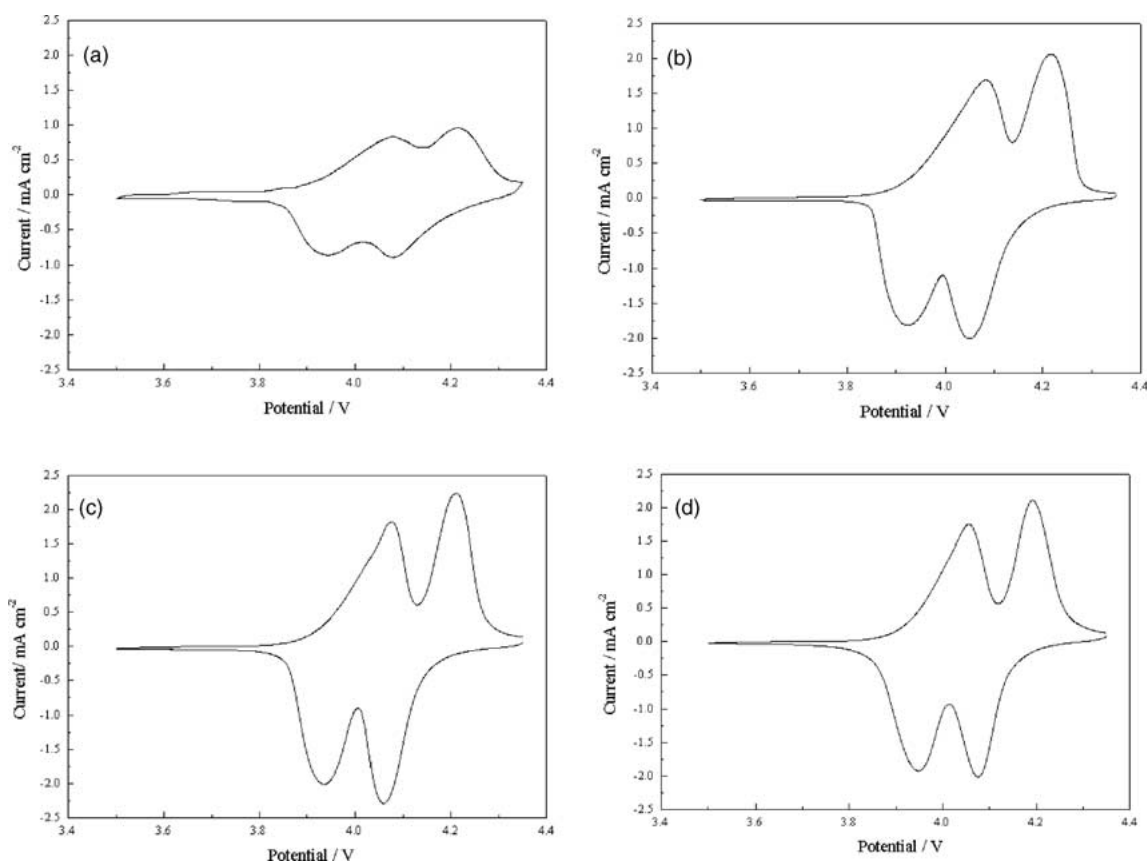


Fig. 7. Cyclic voltammograms of LiMn$_2$O$_4$ samples produced at (a) 250 °C, (b) 650 °C (c) 700 °C and (d) 800 °C with scan rate 0.2 mV s$^{-1}$.

different tetragonal 8a sites in spinel $Li_xMn_2O_4$ ($x < 1$) [16, 17]. The spinel $LiMn_2O_4$ could be formed at low temperature 250 °C, but its redox current peaks were relatively low as shown on curve (a) in Figure 7. The observation reveals that the solid state reaction at 250 °C was not complete. Among them the submicro-sized $LiMn_2O_4$ formed at 700 °C presents the best performance as shown on curve (c): well separated two peaks and with highest peak current. The loss of electrochemical activity of sample formed at 800 °C may be attributed to the structure change. The compound heated at higher temperature may contain some tetragonal $LiMn_2O_4$, which presents less electrochemical activity [18].

### 3.2.2. Charge–discharge properties

Figure 8 presents the effects of $LiMn_2O_4$ formation temperature on the charge and discharge behaviour of button $Li/LiMn_2O_4$ cells. The current density for both processes was 0.2 mA cm$^{-2}$. For most curves there are two distinct potential plateaux at potentials about 4.05 and 4.15 V on charge curves, and 4.10 and 3.92 V on discharge curves, respectively. These potential plateaux correspond to the redox current peaks at the positively or negatively going voltammetry curves in Figure 7. The effect of heating temperature on discharge capacity is shown in Figure 9. From 250 to 550 °C the capacity increases with the increase of heating temperature. In general, the capacity remains constant when temperatures are higher than 550 °C. However, the highest capacity of 128 mAh g$^{-1}$ occurs at 700 °C.

The variations of discharge capacity for Li/1 M LiPF$_6$, EC:DMC = 1:1/$LiMn_2O_4$ button cells during the cycle life test are presented in Figure 10. The cathodic $LiMn_2O_4$ materials were the same as used in Figure 8. The cut-off voltage and charge–discharge current were the same as previously noted. In the range of heating temperature of 250–700 °C the cycle stability increases with the increase of heating temperature. But it decreases
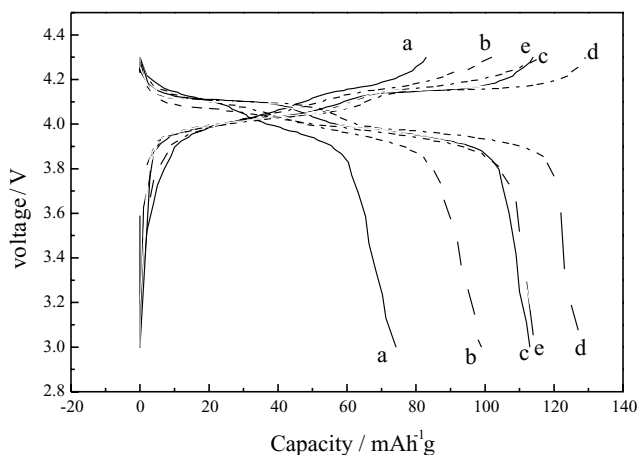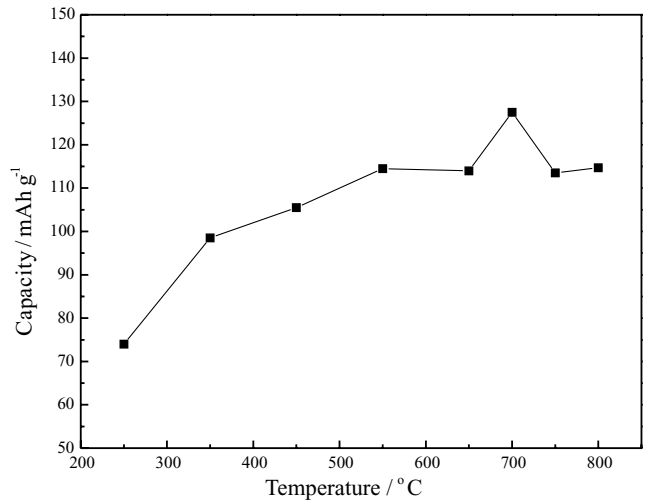


Fig. 9. Effect of heating temperature on the capacity of Li | $LiMn_2O_4$ cells.
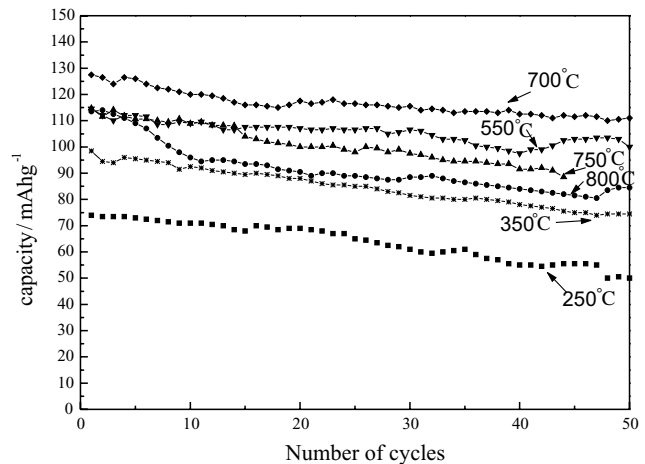


Fig. 10. Variation of discharge capacity of Li | $LiMn_2O_4$ cells during the cycling processes. Heat treatment temperature for $LiMn_2O_4$ samples are indicated.

when the heating temperature rises further. The result shows that the submicro-sized $LiMn_2O_4$ sample synthesized at 700 °C has the best performance with highest capacity and stability. This material may be used in producing rechargeable lithium ion battery. The sol–gel spray-drying method can be applied on an industrial-scale to produce the materials for the lithium ion battery.

## 4. Conclusion

A sol–gel, spray-drying method was used to prepare $LiMn_2O_4$ powder. Via DTA, TGA, IR, XRD and SEM analysis, it was shown that the structure and morphology of $LiMn_2O_4$ powder were strongly affected by the spray speed and the heat treatment temperature. A submicro-sized $LiMn_2O_4$ powder can be produced using a rotating spray speed of 15000 rpm and temperature of 700 °C. The material has an initial capacity of 128 mAh g$^{-1}$ and good cycling ability in 1 M LiPF$_6$,



Fig. 8. Charge and discharge curves of Li | $LiMn_2O_4$ cells. $LiMn_2O_4$ was formed at (a) 250 °C, (b) 350 °C, (c) 550 °C, (d) 700 °C and (e) 800 °C. $I = 0.2$ mA cm$^{-2}$.

EC:DMC = 1:1 solution for the $Li^+$ intercalation reaction. The method may be used on an industrial-scale to produce submicro-sized $LiMn_2O_4$ powder for lithium ion batteries.

## Acknowledgement

## References

1. T. Ohzuku, M. Kitagawa and T. Hirai, *J. Electrochem. Soc.* **137** (1990) 769.
2. Y. Xia, Y. Zhou and M. Yoshio, *J. Electrochem. Soc.* **144** (1997) 2593.
3. A. Momchilov, V. Manev, A. Nassalevska and A. Kozawa, *J. Power Sources* **41** (1993) 305.
4. Y. Shao-Horn, Y. Ein-Eli, A.D. Robertson, W.F. Averill, S.A. Hackney and W.F. Howard, Jr, *J. Electrochem. Soc.* **145** (1998) 16.
5. J. Guan and M.L. Liu, *Solid State Ionics* **110** (1998) 21.
6. S.H. Kang and J.B. Goodenough, *J. Electrochem. Soc.* **147** (2000) 3621.
7. Y. Xia and M. Yoshio, *J. Electrochem. Soc.* **144** (1997) 4186.
8. Y.J. Park, J.G. Kim, M.K. Kim, H.T. Chung and H.G. Kim, *Solid State Ionics* **130** (2000) 203.
9. J.H. Choy, D.H. Kim, C.W. Kwon, S.J. Hwang and Y.I. Kim, *J. Power Sources* **77** (1999) 1.
10. N.J. Dudney, J.B. Bates, R.A. Zuhr, S. Young, J.D. Robertson, H.P. Jun and S.A. Hackney, *J. Electrochem. Soc.* **146** (1999) 2455.
11. D.G. Fauteux, A. Massucco, J. Shi and C. Lampe-Onnerud, *J. Appl. Electrochem.* **27** (1997) 543.
12. Y. Li, C. Wan, Y. Wu, C. Jiang and Y. Zhu, *J. Power Sources* **85** (2000) 294.
13. C.H. Chen, E.M. Kelder, M.J.G. Jak and J. Schoonman, *Solid State Ionics* **86** (1996) 1301.
14. T.J. Richardson, S.J. Wen, K.A. Striebel, P.N. Ross, Jr and E.J. Cairns, *Mater. Res. Bull.* **32** (1997) 609.
15. P. Barboux, J.M. Tarascon and F.K. Shokoohi, *J. Solid State Chem.* **94** (1991) 185.
16. M.M. Thackeray, W.I.F. David, P.G. Bruce and J.B. Goodenough, *Mater. Res. Bull.* **18** (1983) 461.
17. K. Miura, A. Yamada and M. Tanaka, *Electrochim. Acta* **41** (1996) 249.
18. M. Tarascon, W.R. Mckinnon, F. Coowar, T.N. Bowmer, G. Amatucci and D. Guyomard, *J. Electrochem. Soc.* **141** (1994) 1412.